ARTICLE TYPE www. rsc.org/xxxxxx | XXXXXXXX

From isotope labeled CH_3CN to N_2 inside single-walled carbon nanotubes

View Article Online
DOI: 10.1039/C3NR04729F

Christian Kramberger,*[a] Theerapol Thurakitseree,[bc] Erik Einarsson,[bd] Akito Takashima,[e] Toyohiko Kinoshita,[e] Takayuki Muro[e] and Shigeo Maruyama[b]

Received Xth XXXXXXXXXX 20XX, Accepted Xth XXXXXXXXX 20XX
First published on the web Xth XXXXXXXXXX 200X
DOI: 10.1039/b000000x

The observation of one-dimensional N_2 inside single-walled carbon nanotubes raises the questions, how are the N_2 formed and how do they manage to make their way to this peculiar place? We have used N^{15} and C^{13} isotope labeled acetonitrile during the synthesis of single-walled carbon nanotubes to investigate this process. The isotope shifts of phonons and vibrons are observed by Raman spectroscopy and x-ray absorption. We identify the catalytic decomposition of acetonitrile as the initial step in the reaction pathway to single-walled carbon nanotubes containing encapsulated N_2.

1 Introduction

The ability of multi-walled carbon nanotubes (MWNT) to encapsulate N_2 was first demonstrated in Ref. [1]. If N_2 is enclosed in as-synthesized MWNT, the nanotubes exhibit a compartmentalized bamboo structure that traps pockets of N_2.[2,3] The detailed distribution of encapsulated N_2 and N incorporated to the walls of MWNT has been directly imaged by polarized scanning transmission x-ray microscopy.[4] The alignment of N_2 in the confining walls has also been observed by x-ray absorption.[5,6] A commonly observed effect of using N-containing precursors in the growth of single-walled (SW) and MWNT by chemical vapor deposition (CVD) is increased curvature in the emerging sp^2 networks. In MWNT this is seen as topological curvature resulting in the formation of separate compartments. In SWNT, however, reducing diameters increases the geometrical curvature.[7–11]

In the case of MWNT, the N_2 gas is partially aligned on the walls of the nano compartments. For a truly one-dimensional phase of nitrogen, much more narrow single-walled carbon nanotubes with diameters smaller than one nanometer are required. Such configurations of aligned N_2 chains have been predicted and expounded using density functional theory.[12] Only recently was one-dimensional, highly aligned N_2 inside SWNT confirmed by polarized x-ray absorption spectroscopy.[13] The commonly accepted mechanism for the encapsulation of N_2 has been put forth in Ref.[14] Very briefly, C≡N radicals react inside the catalyst particle and release N_2, which then emerges into the currently growing compartment. While the correlation of encapsulated N_2 with the use of N containing precursors is generally accepted, direct identification of the reaction pathway by isotope labeling has not yet been achieved. Moreover, it remains an open issue whether or not the proposed C≡N radicals come from intermediate gas-phase HCN or if they are formed during the catalytic decomposition of CH_3CN.

Here we utilize either CH_3CN^{15} or $CH_3C^{13}N$ to label the pathways of C and N in the proposed intermediate C≡N units. We see that the two inequivalent carbons in CH_3CN are incorporated into the sp^2 network of the SWNT in equal proportion, while the N_2 is formed from the N^{15}. We deduce that the direct catalytic processing of entire CH_3CN molecules at the catalyst surface is the initial step in the reaction pathway leading to N_2-filled SWNT.

2 Materials & Methods

Vertically aligned single-walled carbon nanotubes (VA-SWNT) were grown by no-flow chemical vapor deposition.[10,15] We used either 1.5 vol.% CH_3CN^{15} added to ethanol feedstock or pure $CH_3C^{13}N$ to synthesize vertically aligned SWNT containing N_2^{15} or N_2^{14}. The CH_3CN^{15} and $CH_3C^{13}N$ were purchased from Cambridge Isotope Laboratories, Inc. The isotope purity is given to be >98%. X-ray photoelectron spectra (XPS) were measured with a PHI 5000 VersaProbe setup. X-ray absorption spectroscopy (XAS) was conducted at beamline BL27SU at the SPring-8 synchrotron facility. The beamline is dedicated to soft x-ray absorption spectroscopy.[16,17] To maximize the signal intensity from the encapsulated N_2 molecules (∼600 ppm) we used a slit-limited resolution of 80 meV, a stepsize of 10 meV and acquisition

[a] *University of Vienna, Vienna, Austria. Fax: 43 14277 51375; Tel: 43 14277 72628; E-mail: c.kramberger-kaplan@univie.ac.at*
[b] *University of Tokyo, Tokyo, Japan.*
[c] *Present address: Maejo University, Chiang Mai, Thailand.*
[d] *Present address: University at Buffalo, Buffalo, USA.*
[e] *SPring-8, Sayo, Japan.*

time of 3 s. Additionally, all spectra were recorded at 75° grazing incidence using *p*-polarized x-rays for maximum attainable peak intensities.[13] We normalized the XAS spectra by dividing the drain current of the samples by the simultaneously recorded drain current at the last focusing mirror. To obtain the best possible comparison, N_2^{15} and N_2^{14}@VASWNT were always mounted onto the same sample holder and were always measured without any delay using identical settings.

3 Results & Discussion

3.1 Stoichiometry of N and C

The high yield of N_2 over pyridinic or substitutional N bonding was confirmed by XPS. Figure 1 shows the survey scan of clean, as-synthesized N_2^{15}@VA-SWNT in the lower panel. During the root growth process the CoMo catalyst particles stay attached to the substrate and only pure SWNT emerge upwards. Hence, the single prominent spectral feature is the C1s at 284.6 eV. At this scale the O1s at 530 eV and N1s at 404 eV are hardly discernible. Detailed scans of the N1s and C1s region are shown above the survey scan. The C1s shows an asymmetric Doniach Šunjić lineshape with the secondary π electron shake up. The lineshape is typical for metallicity-mixed SWNT.[18,19] The N1s shows a single prominent peak of molecular N_2 at 404.5 eV. The N1s and C1s were measured with identical resolution settings and can be directly compared. The atomic cross section of nitrogen is 1.8 times that of carbon[20], therefore the abundance of N as compared to C is ∼600 ppm. If we assume a typical macroscopic density of VA-SWNT material to be 50 μg/cm^3, the density of stored N_2 would be equivalent to that of N_2 gas at 340 mbar and 0°C. Inside densely packed SWNT bundles (1.3 g/cm^3) the stored density of N_2 would correspond to that of N_2 gas at 8.8 bar and 0°C. The N/C stoichiometry of 600 ppm is approximately 10 times lower than the 1.5 vol.% of CH_3CN in C_2H_5OH used during SWNT synthesis. The noisy signal just above 401 eV may be tentatively assigned to traces of NO_x. The signal from substitutional or pyridinic N is expected in the range from 398–400 eV, and is evidently not detectable.

3.2 Fractionation of C^{13} and C^{12}

Isotope labeling of the carbons in the feedstock is a viable technique for investigating reaction pathways. We grew SWNT from pure $CH_3C^{13}N$ and regular CH_3CN. The Raman spectra of these two samples are shown in Figure 2.

The high-frequency optical phonon modes undergo a softening and broadening due to the increased mass and phonon-phonon scattering rates.[22–24] The G mode of SWNTs synthesized from pure isotopic $CH_3C^{13}N$, reveals a significant

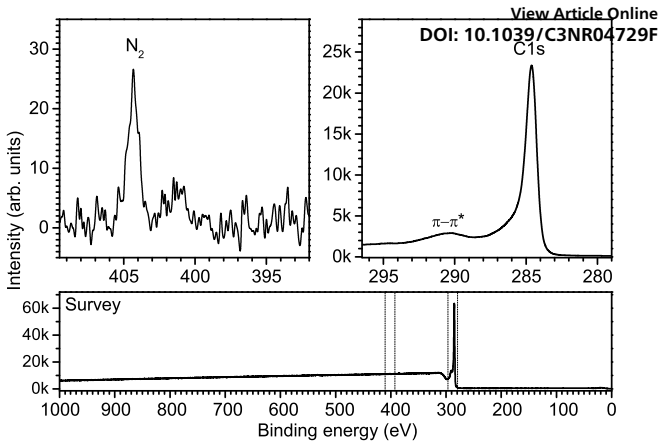

Fig. 1 XPS spectra of N1s (top left), C1s (top right) and survey scan (bottom) of N_2^{15}@VA-SWNT

downshift. The actual concentration of C^{13} can be readily calculated from Eqn. 1

$$\omega(c) = \omega_N \cdot \sqrt{\frac{12+0.011}{12+c}} \qquad (1)$$

Here ω_N is the G-band frequency of naturally occurring C^{12} material , which contains 1.1% C^{13}. The observed maxima of the tangential G modes $\omega_N = 1594.8$ and $\omega(c) = 1564.3$ yield an abundance $c = 48\%$ C^{13} in the nanotube walls. The C^{12} and C^{13} in $CH_3C^{13}N$ have—under the current conditions—roughly the same probability to contribute to growth. The reaction pathways in ethanol were only recently elucidated in a study using site-selectively isotope-labeled C_2H_5OH, where either one or both of the C atoms was replaced with C^{13}. In particular it was demonstrated that under equivalent synthesis conditions the reaction pathway for ethanol is dominated by catalytic decomposition, which has a balanced isotope fractionation.[25]

The even fractionation of both inequivalent C atoms strongly suggests that the entire CH_3CN molecule arrives at the catalytic site, where it is then further processed. We conclude that at 800°C thermal decomposition is negligible since the initial dehydrogenation step is thermally inaccessible.[21] Detailed reaction processes on the catalyst particle during the synthesis are, however, obscured from macroscopic post-synthesis investigations.

In our specific case a scenario may be devised by considering binding energies. The binding energy of C≡N is 891 kJ/mol and that of free C_2 is calculated to be on the order of 300 kJ/mol.[21,26] We suggest that during dissolution the C−C bond and all H bonds in CH_3CN break, after which both C and C≡N diffuse into or on the metal catalyst particle. The inert N_2 is released when two C≡N react. The individual steps

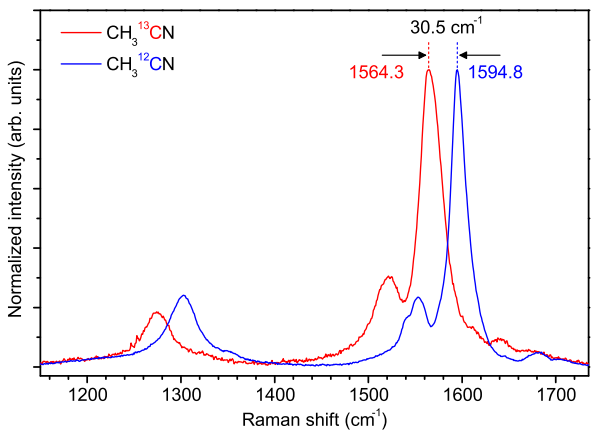

Fig. 2 Raman spectra of SWNT made of natural $C^{13} : C^{12} = 99 : 1$ (blue) and $C^{13} : C^{12} = 48 : 52$ (red). The excitation wavelength is 633 nm

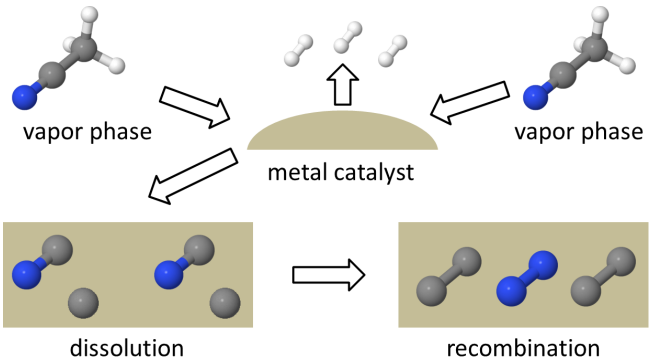

Fig. 3 Steps in the proposed reaction pathway from CH_3CN to dissolved C_2 and inert N_2

are illustrated in Fig. 3. This pathway implies that all the N from CH_3CN is processed via the catalyst particle before it is released as inert N_2.

In the case of pure CH_3CN feedstock there is clearly not enough room inside the SWNT to accommodate all the N_2 that is expelled from the active catalyst particle. Even at sufficiently low concentrations of N, (e.g., less than 3 vol.%, would roughly correspond to the saturation value of 1 at.%) most of the N_2 is released to the environment. The low trapping probability is in accordance with reduced nanotube diameters rooting from larger sized catalyst particles.[10] In the perpendicular growth mode, most of the catalyst particle surface area is not covered by the growing nanotube.[27] Therefore the size of the catalyst particle determines the trapping efficiency for N_2, but it does not determine the diameter of the growing nanotubes.

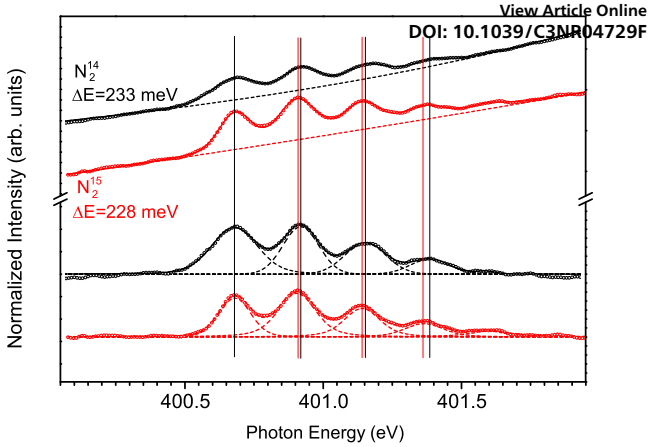

Fig. 4 High resolution XAS of the vibron satellites in the N1s resonance of N_2^{14} (black) and N_2^{15} (red)@VA-SWNT. Raw data are circles, solid lines are fits and dashed lines are individual peaks or the background, respectively.

3.3 Isotope shift in N_2^{15}

X-ray absorption is the method of choice to investigate the possible isotope shift in the vibron energy of N_2. With the natural isotope abundance of over 99% N^{14}, the equidistant satellites in the XAS spectrum are separated by 233±2 meV.[28] For pure N^{15} a spacing of 225±2 meV is expected from scaling with $\sqrt{1/m}$. The isotope shift in the vibrons of isotope mixed $N^{14}N^{15}$ was observed by Raman spectroscopy to be 4 meV.[29] At a full width at half maximum of 140 meV and a typical uncertainty of ±2 meV, very smooth spectra from a ∼600 ppm fraction in the specimen are required to reveal the subtle isotope shift. The XAS spectra in Fig. 4 show the normalized data before and after background subtraction. The lowest resonance energy corresponds to the direct N1s absorption event, and higher resonance energies correspond to concomitant excitation of one or more vibrons. The isotope shift between N_2^{14} and N_2^{15} may already be visible to the trained eye in the original spectra. After subtracting the background, it is much easier to recognize the equidistant series of four well-resolved peaks. A fifth peak is included in the fitting procedure, but its relative weight is considered insufficient for quantitative comparison.

The four Voigtian peaks that are resolved with reliable peak positions reveal an increasing offset due to the isotope shift. The peak positions are marked by vertical lines, and are seen to be systematically shifted to lower resonance energies with increasing vibron numbers. We find an average vibron energy of 228±2 meV , which is in reasonable agreement with the expected value. We are surely at the limit of how accurately the peak positions could be determined from the actual line shapes in one individual spectrum, yet the direct comparison

of the N1s of N_2^{14} and N_2^{15} shows a noticeable isotope shift. The biggest isotope shift is expected for the fourth peak, and would be 24 meV (or halfway between 2 and 3 data points). This corresponds to the shift in peak position that is visible in the actual data and is within experimental accuracy.

The obtained N1s XAS spectra confirm the expected isotope shift of N_2^{14} and N_2^{15}. Moreover, following synthesis and XPS measurement the samples were stored for over six months at ambient conditions until the scheduled beamtime at SPring-8. The extended period over which the N_2^{15} was retained proves that as-grown capped SWNT are tight molecular containers.

4 Conclusions

We used isotope-labeled acetonitrile $CH_3C^{13}N$ and CH_3CN^{15} to trace the reaction pathway from acetonitrile to SWNT containing encapsulated N_2. The balanced incorporation of both inequivalent C atoms in acetonitrile, as evidenced by Raman spectroscopy, is the signature of a catalytic dissolution of the entire molecule. The very strong C≡N bond further suggests that all N is present during dissolution in the catalyst metal. The geometry of a perpendicular growth mode limits the area for encapsulating N_2 that is released when two C≡N react at the catalyst particle. The vibron shift in the N1s x-ray absorption spectra clearly identifies stably encapsulated N_2^{15} from CH_3CN^{15} inside SWNT.

Acknowledgements

Beamtime at SPring-8 was granted for proposal 2013A1107. CK is an APART fellow (Grant No. A-11456) of the Austrian Academy of Science. TT is supported by the office of the higher education commission of Thailand.

References

1 M. Terrones, R. Kamalakaran, T. Seeger and M. Ruhle, Chem. Comm., 2000, 2335–2336.
2 H. C. Choi, S. Y. Bae, W.-S. Jang, J. Park, H. J. Song, H.-J. Shin, H. Jung and J.-P. Ahn, J. Phys. Chem. B, 2005, **109**, 1683–1688.
3 J. Liu, Y. Zhang, M. I. Ionescu, R. Li and X. Sun, Appl. Surf. Sci., 2011, **257**, 7837 – 7844.
4 J. G. Zhou, J. A. Wang, H. Liu, M. N. Banis, X. L. Sun and T. K. Sham, J. Phys. Chem. Lett., 2010, **1**, 1709–1713.
5 A. V. Okotrub, L. G. Bulusheva, A. G. Kudashov, V. V. Belavin, D. V. Vyalikh and S. L. Molodtsov, Appl. Phys. A, 2009, **94**, 437–443.
6 A. V. Okotrub, M. A. Kanygin, L. G. Bulusheva and D. V. Vyalikh, Fullerenes, Nanotubes, Carbon Nanostruct., 2010, **18**, 551–557.
7 P. Ayala, A. Grüneis, C. Kramberger, M. H. Rümmeli, I. G. Solorzano, J. Freire, F. L. and T. Pichler, J. Chem. Phys., 2007, **127**, 184709.
8 E. M. M. Ibrahim, V. O. Khavrus, A. Leonhardt, S. Hampel, S. Oswald, M. H. Rummeli and B. Buchner, Diam Relat Mater, 2010, **19**, 1199–1206.
9 P. Ayala, R. Arenal, A. Loiseau, A. Rubio and T. Pichler, Rev. Mod. Phys., 2010, **82**, 1843–1885.
10 T. Thurakitseree, C. Kramberger, P. Zhao, S. Aikawa, S. Harish, S. Chiashi, E. Einarsson and S. Maruyama, Carbon, 2012, **50**, 2635–2640.
11 T. Thurakitseree, C. Kramberger, A. Kumamoto, S. Chiashi, E. Einarsson and S. Maruyama, Acs Nano, 2013, **7**, 2205–2211.
12 R. E. Barajas-Barraza, J. A. Ramirez-Ruiz and R. A. Guirado-Lopez, Jour. of Comput. Theor. Nanos., 2008, **5**, 2255–2263.
13 C. Kramberger, T. Thurakitseree, H. Koh, Y. Izumi, T. Kinoshita, T. Muro, E. Einarsson and S. Maruyama, Carbon, 2013, **55**, 196–201.
14 J. H. Yang, D. H. Lee, M. H. Yum, Y. S. Shin, E. J. Kim, C. Y. Park, M. H. Kwon, C. W. Yang, J. B. Yoo, H. J. Song, H. J. Shin, Y. W. Jin and J. M. Kim, Carbon, 2006, **44**, 2219–2223.
15 H. Oshima, Y. Suzuki, T. Shimazu and S. Maruyama, Jpn. J. Appl. Phys., 2008, **47**, 1982–1984.
16 H. Ohashi, E. Ishiguro, Y. Tamenori, H. Okumura, A. Hiraya, H. Yoshida, Y. Senba, K. Okada, N. Saito, I. H. Suzuki, K. Ueda, T. Ibuki, S. Nagaoka, I. Koyano and T. Ishikawa, Nuc. Instr. Metho. In Phys. Resea. A, 2001, **467**, 533–536.
17 H. Ohashi, E. Ishiguro, Y. Tamenori, H. Kishimoto, M. Tanaka, A. Irie, T. Tanaka and T. Ishikawa, Nuc. Instr. Metho. In Phys. Resea. A, 2001, **467**, 529–532.
18 C. Kramberger, H. Rauf, H. Shiozawa, M. Knupfer, B. Büchner, T. Pichler, D. Batchelor and H. Kataura, Phys. Rev. B, 2007, **75**, 235437.
19 P. Ayala, Y. Miyata, K. De Blauwe, H. Shiozawa, Y. Feng, K. Yanagi, C. Kramberger, S. R. P. Silva, R. Follath, H. Kataura and T. Pichler, Phys. Rev. B, 2009, **80**, 205427.
20 J. Scofield, J. Electon Spectrosc. Relat. Phenom., 1976, **8**, 129 – 137.
21 A. Lifshitz and C. Tamburu, Int. J. Chem. Kinet., 1998, **30**, 341–347.
22 F. Simon, C. Kramberger, R. Pfeiffer, H. Kuzmany, V. Zólyomi, J. Kürti, P. M. Singer and H. Alloul, Phys. Rev. Lett., 2005, **95**, 017401.
23 C. Kramberger, M. Löffler, M. Rümmeli, A. Grüneis, R. Schönfelder, O. Jost, T. Gemming, T. Pichler and B. Büchner, Phys. Status Solidi B, 2006, **243**, 3050–3053.
24 S. D. Costa, C. Fantini, A. Righi, A. Bachmatiuk, M. H. Rümmeli, R. Saito and M. A. Pimenta, Carbon, 2011, **49**, 4719–4723.
25 R. Xiang, B. Hou, E. Einarsson, P. Zhao, S. Harish, K. Morimoto, Y. Miyauchi, S. Chiashi, Z. Tang and S. Maruyama, ACS Nano, 2013, **7**, 3095–3103.
26 S. Shaik, D. Danovich, W. Wu, P. Su, H. S. Rzepa and P. C. Hiberty, Nat Chem, 2012, **4**, 195–200.
27 M. F. C. Fiawoo, A. M. Bonnot, H. Amara, C. Bichara, J. Thibault-Penisson and A. Loiseau, Phys. Rev. Lett., 2012, **108**, 195503.
28 C. T. Chen, Y. Ma and F. Sette, Phys. Rev. A, 1989, **40**, 6737–6740.
29 M. Musso, F. Matthai, D. Keutel and K. L. Oehme, J Chem Phys, 2002, **116**, 8015–8027.

Graphical Abstract

View Article Online
DOI: 10.1039/C3NR04729F

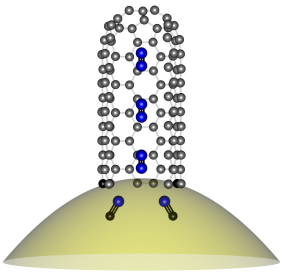

We identify the catalytic decomposition of acetonitrile as the initial step in the reaction pathway to the formation of single-walled carbon nanotubes and the simultaneous encapsulation of N_2.